Author's Accepted Manuscript

Photoelectrochemical TiO_2 nanotube arrays biosensor for asulam determination based on in-situ generation of quantum dots

Jiuying Tian, Yan Li, Jingjiao Dong, Mingjuan Huang, Jusheng Lu

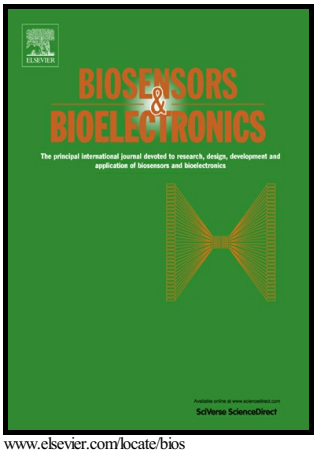

www.elsevier.com/locate/bios

PII: S0956-5663(18)30211-2
DOI: https://doi.org/10.1016/j.bios.2018.03.038
Reference: BIOS10364

To appear in: *Biosensors and Bioelectronic*

Received date: 13 January 2018
Revised date: 16 March 2018
Accepted date: 16 March 2018

Cite this article as: Jiuying Tian, Yan Li, Jingjiao Dong, Mingjuan Huang and Jusheng Lu, Photoelectrochemical TiO_2 nanotube arrays biosensor for asulam determination based on in-situ generation of quantum dots, *Biosensors and Bioelectronic,* https://doi.org/10.1016/j.bios.2018.03.038

This is a PDF file of an unedited manuscript that has been accepted for publication. As a service to our customers we are providing this early version of the manuscript. The manuscript will undergo copyediting, typesetting, and review of the resulting galley proof before it is published in its final citable form. Please note that during the production process errors may be discovered which could affect the content, and all legal disclaimers that apply to the journal pertain.

ACCEPTED MANUSCRIPT

Photoelectrochemical TiO_2 nanotube arrays biosensor for asulam determination based on in-situ generation of quantum dots

Jiuying Tian, Yan Li, Jingjiao Dong, Mingjuan Huang, Jusheng Lu*

Jiangsu Key Laboratory of Green Synthetic Chemistry for Functional Materials, School of Chemistry and Materials Science, Jiangsu Normal University, Xuzhou 221116, PR China

*Corresponding author at: School of Chemistry and Materials Science, Jiangsu Normal University, 101 Shanghai Road, Xuzhou 221116, PR China. Tel.: +86-516-83403165. jushenglu@jsnu.edu.cn (J. Lu)

Accepted manuscript

Abstract

Inspired by the photoelectrochemical (PEC) properties of TiO_2 nanotubes arrays (TNA) and their application as a super vessel for immobilizing biomolecules, we constructed an inhibition-effect PEC biosensor for determination of asulam based on the in-situ generation of CdS quantum dots (QDs) on TNA using an enzymatic reaction. Horseradish peroxidase (HRP) enzyme was covalently assembled on the inner-wall of TNAs, which exhibited good electrochemical and catalytic properties. In the mixture solution containing H_2O_2, CdY and $S_2O_3^{2-}$, HRP enzyme in TNAs catalyzed H_2O_2 reduce $S_2O_3^{2-}$ to S^{2-}. The generated S^{2-} reacted with CdY to form CdS QDs in situ on the TNAs, improving the PEC performance of TNA under visible light irradiation. The photocurrent would decrease after addition of asulam due to its inhibitory effect

ACCEPTED MANUSCRIPT

towards HRP enzyme activity. Under the optimal experimental conditions, the constructed PEC TNA/HRP biosensor exhibited a satisfying linear range (0.02-2.0 ng mL^{-1}), low limit of detection (4.1 pg mL^{-1}) and good selectivity towards asulam determination, and has been successfully applied for the analysis of real environmental water samples with good accuracy of the recoveries ranged from 90 to 114%.

Keywords: Asulam; Enzymatic inhibition; Photoelectrochemical biosensor; QDs generation in-situ.

1. Introduction

Enzymes are exquisite biocatalysts mediating every biological process in living organisms, which do not freely diffuse within the cytosols, but are spatially defined within subcellular organelles (Schoffelen and van Hest, 2012; Conrado et al., 2008; Yan et al., 2009). Inspired by natural enzyme architectures, researchers have long directed their attention to the construction of enzyme complexes, which pushed the development for micro-/nanoscale enzymatic reactors with confined space using smart nanostructured materials (Liu et al., 2013; Fu et al., 2012; Shangguan et al., 2017). In our previous works, we successfully assembled the cytochrome P450 enzyme in TiO_2 nanotube arrays or macroporous silica foams which exhibited excellent enzymatic activity and catalytic effect toward the drug metabolism process (Lu et al., 2014, 2016).

TiO_2 nanotubes arrays (TNAs), one of the most extensively studied porous nanodevices, can be synthesized by electrochemical anodization on titanium foils in fluoride-based electrolyte with

Accepted manuscript

ACCEPTED MANUSCRIPT

good uniformity, controllable pore size, and good mechanical adhesion strength (Paramasivam et al., 2012; Roy et al., 2011; Jun et al., 2012; Tan et al., 2012; Ghicov et al., 2009). TNAs possess remarkable physical and chemical properties, and have applied for super-capacitors, drug delivery, and photocurrent conversion (Song et al., 2009; An et al., 2010; Pardo-Yissar et al., 2003; Chen et al., 2010). Furthermore, the large surface area, one-dimensional nanostructure with tubular symmetries, good biocompatibility, and chemical stability are advantages that make TNAs an excellent microenvironment for immobilization of biomolecules with increasing quantity and bioactivity (Zhang et al., 2011; Wang et al., 2010; Lai et al., 2013; Liu et al., 2009). In addition, as a semiconductor, vertically aligned TNAs have been applied in the photoelectrochemical (PEC) sensors owing to their excellent photochemical property (Zhang et al, 2008), which can offer a large interior and outer surface area and provide a direct pathway for the transfer of photoexcited electrons, leading to the enhancement of light absorption and carrier separation (Li et al., 2015). Nevertheless, it is a pity that the poor response to visible light of TiO_2 caused by its wide band gap (E_g=3.2 eV) (Tachikawa et al., 2011), and the fast recombination of photogenerated electron-hole pairs had significantly hindered the application of pure TiO_2 in photocatalysis (Chen and Mao, 2007), limiting its some PEC applications. Various functional materials, such as quantum dots (QDs) (Wang et al., 2012; Yan et al., 2010; Liang et al., 2012; Sun et al., 2008; Ouyang et al., 2012), metal or metal oxides (An et al., 2010; Wang et al., 2012; Kang and Park, 2013) have been combined with TNAs to extend their PEC biosensing application. Most of QDs were generally functionalized on TNAs by pre-synthesis or heterogeneous synthesis in the previous reports (Liang et al., 2012; Ouyang et al., 2012). However, the use of pre-synthesized QDs in PEC platforms is frequently limited by high background signals due to nonspecific adsorption of QDs

Accepted manuscript

ACCEPTED MANUSCRIPT

on surfaces, which is unfavorable for PEC detection (Freeman and Willner, 2009). The enzymatic in-situ generation of QDs is a promising substitute for the use of a pre-synthesized semiconductor (Malashikhina et al., 2013).

Asulam (methyl 4-aminobenzene sulfonyl carbamate) is a pesticide with a widely broad spectrum of biological activity, acting by stopping the cell division and growth of plant tissues (Sanchez et al., 2008). Due to the high solubility in water and soil, it can accumulate and remain in environment, justifying the development of suitable analytical methods. Asulam has been determined by several analytical methods, including chromatography (An et al., 2011; Li et al., 2011; Chicharro et al., 2002), fluorescence (Subova et al., 2006; Nakamura et al., 2000), chemiluminescence (Sanchez et al., 2008; Chivulescu et al., 2004) and electrochemical methods (Chicharro et al., 2008; Nouws et al., 2002). Herein, inspired by the increasing application of TNAs as a super vessel for immobilizing biomolecules (Lu et al., 2014; Chen et al., 2010) and excellent performance of enzymatic in-situ generation of QDs, we covalently assembled horseradish peroxidase (HRP) enzyme on the inner-wall of TNAs and constructed a nanotube array enzymatic biosensor (TNA/HRP) for asulam determination. In details, when the constructed TNA/HRP biosensor was immersed in a mixture solution containing H_2O_2, CdY and $S_2O_3^{2-}$, HRP enzyme in TNAs could catalyze the reduction of $S_2O_3^{2-}$ to S^{2-} in the presence of H_2O_2. The generated S^{2-} reacted with CdY to form CdS QDs in situ on the TNAs, so the PEC performance of TNA would improve under visible light irradiation because of the existence of CdS (Scheme 1). However, when the TNA/HRP biosensor was immersed in the above solution containing asulam, the PEC signal of TNA would decrease due to the inhibition of asulam to the HRP enzyme (Sanchez et al., 2008). With the increase of asulam concentration, the amount of CdS generated

Accepted manuscript

in-situ on TNAs decreased significantly, leading to the decrease of photocurrent. Based on this, a PEC TNA/HRP biosensor for the sensitive determination of asulam was constructed.

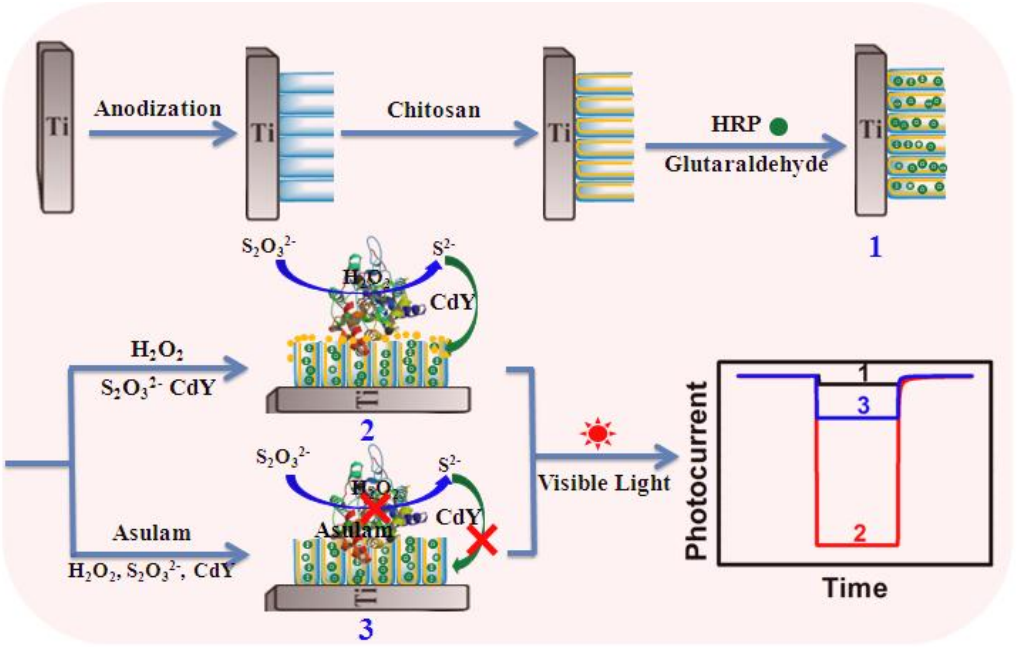

Scheme 1. The construction of TiO_2 nanotube array enzymatic bioreactor and in-situ synthesis of CdS QDs

2. Experimental

2.1. Materials and Reagents

Titanium foils (99.7% purity) with a thickness of 0.127 mm, horseradish peroxidase (HRP, E.C. 1.11.1.7, ≥250 U mg^{-1}, from Horseradish), asulam, chitosan (low molecular weight, 85% deacetylation) and glutaraldehyde were purchased from Sigma-Aldrich Co. Ltd. (St. Louis, MO, USA). Ethylenediaminetetraacetic acid cadmium salt (CdY), H_2O_2 and $Na_2S_2O_3$ were obtained from Sinopharm Chemical Reagent Co., Ltd. (Shanghai, China). Phosphate buffer solution (PBS, 0.1 M, pH 7.4) was prepared by mixing the stock solution of K_2HPO_4 and KH_2PO_4. All other chemicals were of at least analytical grade and used as received. Deionized water (18.2 MΩ cm) obtained from a Milli-Q water purification system was used in all measurements.

2.2. Apparatus

ACCEPTED MANUSCRIPT

The scanning electron micrographs were recorded with a field emission scanning electron microscope (FESEM, Hitachi S-4800, Japan). Transmission electron microscopy (TEM) was performed on a JEM-2100 transmission electron microscope (JEOL, Japan) at an acceleration voltage of 200 kV. X-ray photoelectron spectroscopy (XPS) was conducted on a Thermo ESCALAB 250XI instrument with Al Kα X-ray source. All binding energies were calibrated with surface adventitious carbon of 284.8 eV. UV-vis absorption spectra were measured on a UV-2450 spectrometer (Shimadzu, Japan). Fluorescence spectra were measured on an F-4600 FL spectrophotometer (Hitachi, Japan). PEC measurements were carried out on a CHI660E electrochemical workstation (CH Instruments, Austin, USA), in which, a conventional three-electrode system composing of a modified Ti/TNAs as the working electrode, a saturated calomel electrode (SCE) as the reference electrode and a platinum wire electrode as the counter electrode, respectively. A 500 W Xe lamp was used as an irradiation source fitted with a 400 nm UV filter (Zolix, China) and a mechanical shutter was used to control the light on and off.

2.3. Fabrication of TiO_2 Nanotube Arrays (TNAs) and construction of TNA/HRP biosensor

The TiO_2 nanotube arrays (TNAs) on titanium foil were fabricated by the electrochemical anodization technique according to our previous work (Lu et al., 2014). For construction of TNA/HRP biosensor, the prepared TNAs was firstly immersed in 2 mL of 0.1 wt% chitosan (CS) solution, which was dissolved in 1.0 wt% acetic acid solution, at room temperature (RT) for 4 h with gentle stirring. After rinsing with water, the above TNA/CS was immersed in 1.0 mL of 0.1 M pH 7.4 PBS containing 1.0 wt% glutaraldehyde solution for 2 h, followed by incubating with 1.0 mL of 0.1 M pH 7.4 PBS containing 1.0 μM HRP at RT for 1 h and 4 ^{o}C overnight in a 100% moisture-saturated environment. After rinsing with 0.01 M pH 7.0 PBS, the TNA biosensor

Accepted manuscript

assembled with HRP enzyme (TNA/HRP) was constructed and stored at 4 ^{o}C for the following use.

2.4. PEC measurement for asulam determination and real sample analysis

Before PEC measurement, the TNA/HRP was firstly immersed in a 0.1 M pH 7.4 PBS containing 0.1 mM $S_2O_3^{2-}$, 5 μM CdY, 0.1 mM H_2O_2, and asulam with different concentrations, kept for 15 min to form CdS QDs in situ on the TNAs (TNA/CdS). Then the fabricated TNA/CdS was used as working electrode for PEC measurement in an electrolyte solution, in which, 0.1 M ascorbic acid was used as electron donor and added in 0.1 M Na_2SO_4 solution. The concentration of asulam could be determined by the measured photocurrent value *I*.

The water samples were lake water, river water and drinking water, respectively, which were collected from Yunlong Lake, Yuquan River and local supermarket, respectively. Each water sample was filtered through a filter paper, and stored at 4 ◦C, which was used for the PEC measurement to determine the concentration of asulam by TNA/HRP biosensor. At the same time, a recovery test was carried out in accordance with the same procedure to demonstrate the validity of the proposed biosensor. Blank sample was spiked with different amount of asulam standard solutions to produce a series of spiked solutions respectively.

3. Results and discussion

3.1. Construction and characterization of TNA/HRP biosensor and enzymatic generation of CdS QDs in situ

To construct a TNA/HRP enzymatic biosensor and investigate the electrochemical and enzymatic activity of HRP enzyme confined in the nanotubes, TNAs were fabricated by electrochemical anodization technique. The SEM results showed that (Fig. 1A), when the

Accepted manuscript

anodization potential was 20 V at an anodization time of 4 h, the prepared nanotube of TNAs had an average length of 3.5 μm and the inner diameter of ~100 nm.

For covalent assembly of HRP enzyme on the inner-wall of TNAs, chitosan (CS), a natural-biopolymer with excellent capability for film formation and biocompatibility, has a large number of primary amine at the C-2 position of the glucose amine residues (Muzzarelli, 2009), was uniformly coated on the inner wall of TNAs. The assembly of HRP enzyme on the inner-wall of TNAs could be monitored by the electrochemical impedance spectroscopy (Fig. S1A). The charge transfer resistance (R_{ct}) after each assembling step varied in the following order: Ti foil (25 Ω) < Ti/TNA (120 Ω) < Ti/TNA/CS (285 Ω) < Ti/TNA/CS/HRP (520 Ω), confirming the successful construction of the TNA/HRP biosensor, and the total assembly amount of HRP in the TNAs was determined by Bradford method (Bradford, 1976) to be1.21±0.06 pmol cm^{-2}. In addition, the change of redox peak currents of probe $Fe(CN)_6^{4-/3-}$ in cyclic voltammograms also confirmed the successful construction of the TNA biosensor (Fig. S1B).

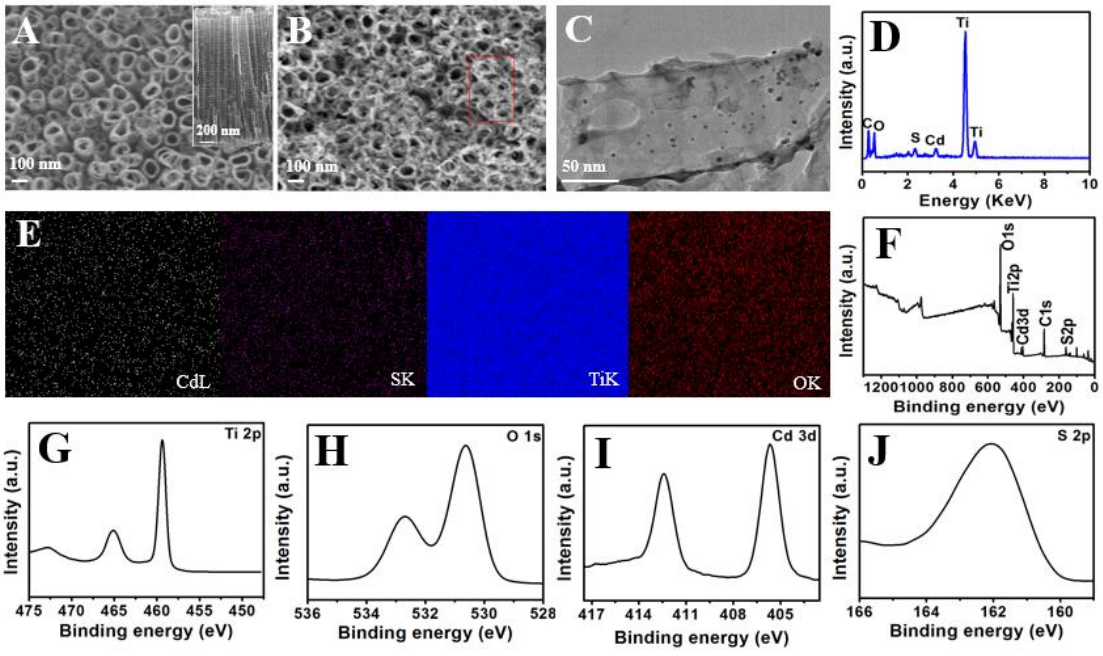

Fig. 1. (A) FESEM top-view image of TNAs and corresponding cross section image (Inset); FESEM top-view image (B) and TEM image (C) of TNA/CdS; Energy dispersive spectroscopy (EDS) of TNA/CdS (D) and

ACCEPTED MANUSCRIPT

corresponding element distribution mapping of Cd, S, Ti and O (E). XPS survey spectrum of TNA/CdS (F) and high-resolution XPS spectra of Ti 2p (G), O 1s (H), Cd 3d (I) and S 2p (J).

After immersing the TNA/HRP in 0.1 M pH 7.4 PBS containing $S_2O_3^{2-}$, H_2O_2 and CdY, some nanoparticles with the size of 3-6 nm were observed not only on the mouth of TNAs but also in the nanotube of TNAs from the SEM and TEM images (Fig. 1B and C). The energy dispersive spectroscopy (EDS) and corresponding element distribution mapping (Fig. 1 D and E) showed the existence of Cd, S, Ti and O, in which, the area ratio of Cd and S was 1:1, confirming the in-situ generation of CdS. In addition, the surface composition and chemical state of TNA/CdS could be further proved by a XPS measurement. Fig. 1 F to J showed the XPS survey spectrum of TNA/CdS and corresponding high-resolution XPS spectra of Ti 2p, O 1s, Cd 3d and S 2p. The characteristic binding energy values of 459.4 and 465.1 eV for Ti $2p_{3/2}$ and Ti $2p_{1/2}$, respectively, indicated a Ti^{4+} oxidation state originating in TiO_2 (Fig. 1G) (Su and Liu, 2011). Similarly, the O 1s spectra in Fig. 1H was divided into two peaks with binding energies of 530.6 and 532.7 eV, which were attributed to the crystal lattice oxygen of Ti-O in TiO_2 and surface hydroxyl groups, respectively (Chen et al., 2013). The peaks at 405.7 and 412.3 eV (Fig. 1I) were ascribed to the Cd $3d_{5/2}$ and Cd $3d_{3/2}$ states of Cd^{2+} in CdS, respectively (Zhang et al., 2012). Furthermore, a single peak at 162.1 eV in Fig. 1J was observed, which was attributed to the presence of S^{2-} (Li et al., 2012). All of the XPS results further suggested the in-situ generation of CdS on the TNAs.

After ultrasonic treatment of TNA/CdS slightly for 10 min, the TEM image, UV-vis absorption spectroscopy and fluorescence spectroscopy of the obtained suspension showed that, CdS QDs could be dispersed in aqueous solution with an average size of 5 nm (Fig. 2A), and had a typical absorption peak at 428 nm. Furthermore, a fluorescence emission peak was observed at 546 nm under the excitation of 420 nm (Fig. 2B), which indicate that the electron transfer from the valence

Accepted manuscript

band (VB) to the conduction band (CB) of QDs would be easy to occur under visible light irradiation and generate electron-hole pairs. Under visible light irradiation, no significant photocurrent was observed for TNAs (curve a of Fig. 2C) due to the CB and VB of TNA at -4.21 and -7.41 eV, respectively, and its band gap was 3.2 eV, which could only utilize the UV light irradiation (Tachikawa et al., 2011). However, a typically anodic photocurrent could be observed for TNA/CdS at an applied potential of +0.2 V (curve b of Fig. 2C). It was because that, the band gap of CdS QDs was calculated to be 2.89 eV according to the UV-vis absorption spectrum (Fig. 2B). Coupled with the information that the formal redox potential peak of CdS QDs was observed at -0.83 V (vs. SCE, inset of Fig. 2B), the CB and VB positions of CdS QDs could be quantified to be -3.90 eV and -6.79 eV, respectively. Under visible light irradiation, CdS QDs excited electrons from the CB to the VB and generated holes at the VB. Because the CB of TNAs was more positive than that of CdS QDs, the excited electrons could quickly transfer from the CB of CdS QDs to that of TNAs, resulting in the generation of photocurrent. Furthermore, the tubular structure of TNAs was helpful for separating and transferring photoinduced electrons to the titanium substrate foil (Zhang et al., 2009), which contributed to the increasing photocurrent.

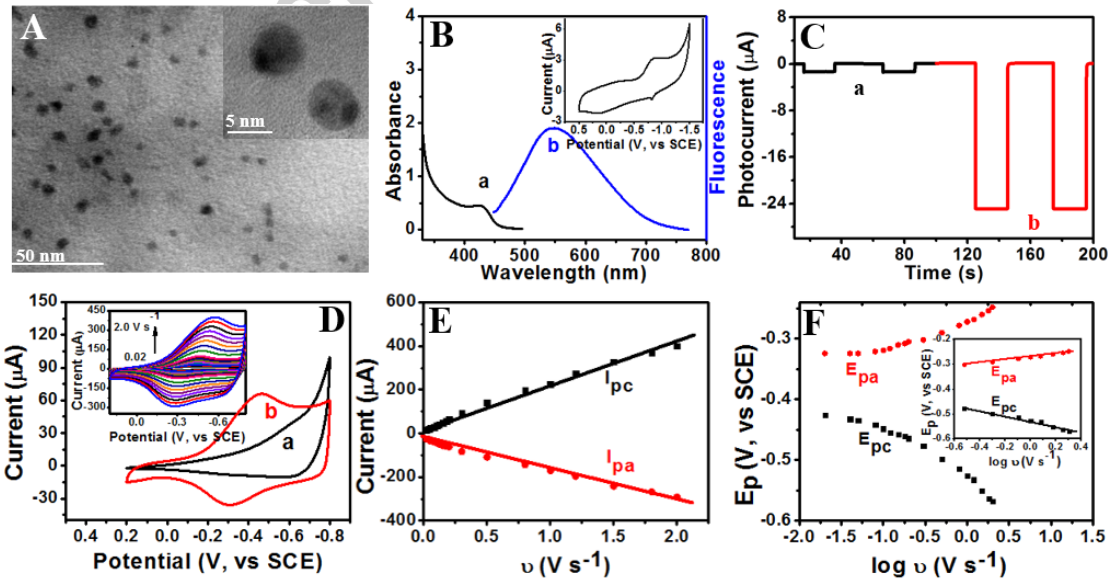

ACCEPTED MANUSCRIPT

Fig. 2. (A) TEM and HRTEM (Inset) image of CdS QDs; (B) UV-vis (a) and fluorescence (b) spectra of CdS QDs, Inset: Cyclic voltammograms of CdS at GCE in 0.1 M pH 7.4 PBS; (C) Photocurrent responses of different systems: (a) TNA, (b) TNA/CdS; (D) Cyclic voltammograms of Ti/TNA (a) and Ti/TNA/HRP (b) in 0.1 M pH 7.4 PBS at scan rate of 0.1 V s^{-1}, Inset: Cyclic voltammograms of Ti/TNA/HRP at different scan rates range from 0.02 to 2.0 V s^{-1}; (E) Plot of the peak current versus the scan rate (υ); (F and inset) Plot of the peak potential versus logυ.

3.2. Electrochemical performance of HRP enzyme in the TNA

The reason for in-situ generation of CdS QDs may be due to the excellent electrochemical and catalytic properties of HRP enzyme. In 0.1 M pH 7.4 PBS solution at the scan rate of 0.1 V s^{-1}, a pair of redox peaks was observed for TNA/HRP with cathodic peak at -0.452 V and the corresponding anodic peak at -0.317 V (Fig. 2D), confirming that the redox response of HRP resulted from the direct electron transfer between the heme electroactive site of HRP enzyme and the Ti/TNA. In addition, cyclic voltammogram of HRP enzyme showed a strong dependence on solution pH value, as shown in Fig. S2A. The peak potentials were observed with an increase in solution pH value from 5.1 to 9.9, which indicated that the hydrogen ions took part in the electrode reaction. The slope of the peak potentials versus pH value was 53.6 mV pH^{-1} (Fig. S2B) (R^2 = 0.9968), which was close to the Nernst's value of 59.2 mV pH^{-1}, indicating the participation of H^+ and the number of electron transfer in the redox process was one. With the increase of scan rate from 0.02 to 2.0 V s^{-1}, both the cathodic peak and anodic peak currents all increased (Inset of Fig. 2D), which varied linearly with the scan rates (Fig. 2E), indicating a surface-controlled process (Myland and Oldham, 2005). Furthermore, the anodic and cathodic peak potentials were linearly depended on the logarithm of scan rate (υ) when the υ was higher than 0.3 V s^{-1} (Fig. 2F and inset). Based on the Laviron's method (Laviron, 1979), the electron transfer coefficient (α) was calculated to be 0.36, The electron transfer rate constant (K_s) of HRP enzyme was calculated

Accepted manuscript

ACCEPTED MANUSCRIPT

to be 2.66 s^{-1} at a scan rate of 0.5 V s^{-1} which indicated the Ti/TNA could provide a fast electron transfer pathway and a favorable microenvironment for the assembled HRP enzyme. Furthermore, when H_2O_2 was added in the 0.1 M pH 7.4 PBS electrolyte solution, the CV curve shape of TNA/HRP changed with the increase of the cathodic peak current at -0.452 V (vs. SCE) (curve b of Fig. S3), suggesting a typically electrocatalytic H_2O_2 reduction process. Addition of H_2O_2 into the electrolyte solution led to the increase of the cathodic current, which could be attributed to the electrocatalysis of HRP (curve c-e of Fig. S3).

3.3. Enzymatic kinetic performance of HRP enzyme in TNAs with different dimensions

To study the catalytic activity of HRP enzyme in different confined spaces, the TNAs with different dimensions were prepared by regulating the anodization potential within the range of 10-40 V and fixing anodization time for 4 h according to our previous work (Lu et al., 2014). As seen from Fig. 3, for the TNA1 with small tube diameter (~50 nm), the diffusion of substrates, such as $S_2O_3^{2-}$ and H_2O_2, into the nanotube of TNAs would be hindered due to the steric inhibition, and for the TNA4 with relatively large tube diameter (~200 nm), substrates $S_2O_3^{2-}$ and H_2O_2 in the TNAs easily diffused into the surrounding milieu, which all would lead to the decrease of the substrate amount in the TNAs, resulting in the decrease of the amount of S^{2-} catalyzed by HRP enzyme and the decrease of generated CdS (Fig. 3 A and D). Only for the TNA2 or TNA3 with appropriate tube diameter (~100 and 150 nm), the transportation of the substrate from the bulk solution into the TNAs, and the diffusion of the product from the nanotube to the bulk solution would be improved, so the amount of CdS generated in-situ in the TNA would increase (Fig. 3 B and C). In which, the amount of CdS was the most for TNA2. Similarly, for the different TNAs, the change trend of photocurrent of TNA after generating CdS in-situ was also the same (curve a-d

Accepted manuscript

of Fig. 3E).

Meanwhile, the tube diameters of TNAs had a great influence on the enzymatic activity of HRP enzyme. By increasing the tube diameter of TNAs from 50 to 100 nm, the enzymatic reaction rate of HRP (photocurrent) increased. Upon further increase of the tube diameter of TNAs from 100 to 200 nm, the enzymatic reaction rate of HRP decreased (Fig. 3F). Furthermore, by increasing the tube diameter, the collision frequency between enzyme and substrate in the TNAs increased, the enzymatic rate constant k_{cat} increased and reached a maximum value for TNA2. Upon further increase of the tube diameter, the k_{cat} decreased (Inset of Fig. 3F). In addition, with the increase of tube diameter of TNAs, the apparent Michaelis constant K_m^{app} increased.

The possible reason is that, when the enzyme was confined in TNAs with small tube inner diameters (confined spaces), the confinement effect facilitated the maintenance of bioactivity and the high affinity toward substrate of immobilized enzyme (Chen et al., 2009). When immobilized on a relatively large space, the enzymatic activity and affinity of the enzyme to substrate would decrease. In addition, as shown in the inset of Fig. 3F, the enzymatic efficiency of k_{cat}/K_m^{app} had the same trend as the enzymatic rate constant k_{cat}. Therefore, we could conclude that the CdS QDs generated on TNAs was due to the enzymatic performance of HRP in TNAs, and the appropriate tube diameter of TNAs, such as ~100 nm, could guarantee the effectively catalytic activity of HRP enzyme. The HRP enzyme spatially confined in the TNAs exhibited excellent enzymatic activity and catalytic efficiency because of the confinement effect of TNAs, the k_{cat} and k_{cat}/k_m^{app} were 6.36 s^{-1} and 1.74 μM^{-1} s^{-1} for TNA2, respectively.

Accepted manuscript

ACCEPTED MANUSCRIPT

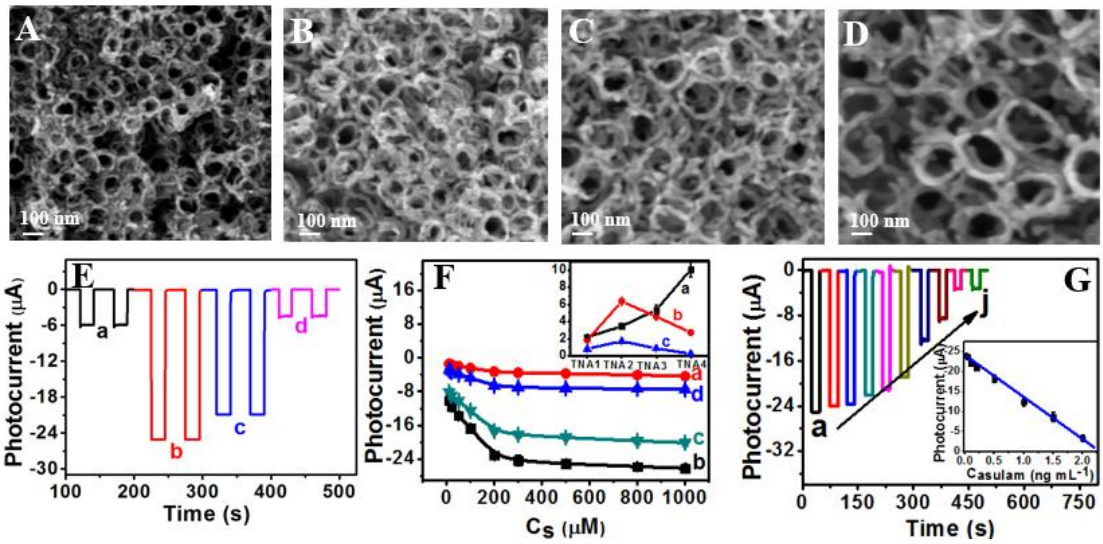

Fig. 3. (A, B, C, D) FESEM image of CdS on the TNA1, TNA2, TNA3 and TNA4; (E) Photocurrent responses of different systems: (a) TNA1/CdS, (b) TNA2/CdS, (c) TNA3/CdS, (d) TNA4/CdS; (F) Michaelis–Menten plots of enzymatic reactions that occurred inside the different TNAs, (a) TNA1, (b) TNA2, (c) TNA3, (d) TNA4, Inset: Corresponding kinetic parameters for the enzymatic reactions with different TNA, (a) K_m^{app}, μM, (b) k_{cat}, s^{-1}, and 1.74 (c) k_{cat}/K_m^{app}, μM^{-1} s^{-1}; (G) Photocurrent responses of TNA/HRP biosensor under visible light irradiation after immersing in 0.1 M pH 7.4 PBS solution containing 0.1 mM $S_2O_3^{2-}$, 5 μM CdY, 0.1 mM H_2O_2 and asulam with 0 (a), 0.02 (b), 0.05 (c), 0.10 (d), 0.20 (e), 0.50 (f), 1.0 (g), 1.5 (h), 2.0 (i) and 3.0 ng mL^{-1} (j), respectively. Inset: Calibration curve of photocurrent response change of the biosensor versus asulam concentration in the ranges of 0.02 to 2.0 ng mL^{-1}. Applied potential, +0.2V.

3.4. Optimization of experimental conditions on the TNA/HRP biosensor

The applied potential played an important role in PEC biosensing since the bias potential affects the recombination probability of the photogenerated electrons/holes. As shown in Fig. S4A, the photocurrent response of the biosensor increased with changing the bias potentials from 0 to +0.6 V, indicating that the photo-induced electrons were effectively driven to the working electrode by the positive bias potential that was beneficial to charge separation. Therefore, to avoid the interference of other reductive species coexisting in the samples at high positive potential, +0.2 V was considered as the optimized bias potential applied on the biosensor. The medium pH affects both the enzyme activity and the optimum of operating potential in case of the substrates electron

Accepted manuscript

ACCEPTED MANUSCRIPT

transfer. The photocurrent response was measured in the range of pH 4.0-9.0 in 0.1 M PBS. The results showed that (Fig. S4B), the photocurrent response increased at first with increasing pH of solution, the maximum response was obtained at pH 7.0. But the photocurrent decreased when the pH was larger than 8.0. So, 0.1 M PBS solution with pH 7.4, a physiological pH value, was used in the experiments. In addition, the influence of the incubation time on the response of the PEC biosensor was investigated (Fig. S4C), the photocurrent leveled off after 30 min, which indicating that the reaction attained its maximum. Thus, 30 min was selected as the incubation time for the PEC biosensor. Furthermore, the contents of H_2O_2 were assessed to obtain an optimal PEC response for the system (Fig. S4D). The photocurrent increased with the increase of H_2O_2 concentration in 0.1 M pH 7.4 PBS, the photocurrent significantly increased. The photocurrent response achieved a plateau in the presence of 0.1 mM H_2O_2 and increased slightly thereafter. Accordingly, a 0.1 mM of H_2O_2 was selected for the enzyme-catalyzed reaction.

3.5. Determination of asulam by TNA/HRP biosensor

Based the excellent enzymatic activity of HRP enzyme confined in TNA nanotubes and excellent confinement effect of TNA, we constructed a PEC TNA/HRP biosensor for asulam determination. The TNA/HRP biosensor was firstly immersed into a mixed solution containing 0.1 mM $S_2O_3^{2-}$, 5 μM CdY, 0.1 mM H_2O_2 and asulam with different concentrations for 30 min. The results showed that (curve a-i of Fig. 3G), the photocurrent significantly decreased with the increase of asulam concentration due to the inhibitory effect of asulam towards HRP enzyme (Sanchez et al., 2008). Under the optimal experimental conditions, the decrease value of photocurrent was dependent on the asulam concentration, which was linear proportional to the concentration of asulam in the ranges of 0.02 to 2.0 ng mL^{-1}, the linear regression equation was I =

Accepted manuscript

ACCEPTED MANUSCRIPT

10.24C (ng mL^{-1})-23.51 (R^2=0.9941) (Inset of Fig. 3G), and a limit of detection (LOD) of such biosensor based on a signal-to-noise ratio of 3 was 4.1 pg mL^{-1}, which indicated the TNA/HRP could be used as a potential biosensor for determining target. Compared to other assays summarized in Table 1, the proposed method for asulam determination exhibited a satisfying linear range and limit of detection.

Table 1 Comparison of the proposed method for asulam biosensing with other previously reported works

Methods	Linear range (μg L^{-1})	LOD (μg L^{-1})	Reference
Photochemiluminometry	70-5000	40	Chivulescu et al., 2004
GC-MS	5-500	5.0	An et al., 2011
DLLME spectrophotometry	1.0-80.0	0.18	Eskandari and Shahbazi-Raz, 2016
Electrochemical	2300-20700	2.76 (FIA)	Nouws et al., 2002
FIA-fluorometry	5-15000	5.0	Subova et al., 2006
MEKC	1000-25000	400	Chicharro et al, 2002
FIA-chemiluminescence	0.36-35	0.12	Sanchez t al., 2009
Fluorometry	20-300	20	Nakamura et al., 2000
PEC biosensor	0.02-2.0	0.0041	This work

In addition, some common herbicides, such as 2, 4, 6-trichlorophenol, phenol, paraquat, atrazine, amitrole and 2, 4, 5-T (2, 4, 5-trichlorophenoxyacetic acid) were introduced as control. As shown in Fig. S5, compared with the target, no apparent change of photocurrent by the assay was observed, even at a higher concentration (10.0 μg mL^{-1}) than that of asulam (2.0 ng mL^{-1}), which indicated the high selectivity of the proposed method. Furthermore, to evaluate analytical reliability and application potential of the proposed TNA/HRP PEC biosensor, the concentration of asulam in real environmental water sample (lake, river or drinking water) was determined and the spiked experiment was carried out. As seen in Table 2, the relative standard deviation values of the analytical results were between 3.5-6.3%, and the recoveries for the spiked samples ranged from 90% to 114%, which implied the PEC biosensor had a good accuracy in a wide linear range and was fully applicable to the real sample analysis.

Accepted manuscript

ACCEPTED MANUSCRIPT

Table 2 Determination of asulam with the proposed PEC biosensor

Sample	Spiked (ng mL^{-1})	Found (ng mL^{-1})	Recovery (%)	RSD (%, n=6)
Lake water	0.00	0.03	--	6.3
	0.10	0.14	110	4.5
	1.00	1.11	108	3.9
	2.00	1.95	96	3.5
River water	0.00	ND	--	--
	0.10	0.09	90	4.9
	1.00	1.04	104	4.1
	2.00	2.13	107	3.8
Drinking water	0.00	ND	--	--
	0.10	0.10	100	5.7
	1.00	1.14	114	4.7
	2.00	1.97	99	3.9

Conclusions

In the present work, an inhibition-effect PEC biosensor for determination of asulam was constructed based on the in-situ enzymatic generation of CdS QDs on TNA. HRP enzyme, which was covalently assembled on the inner-wall of TNAs, exhibited good electrochemical and catalytic properties due to the confinement effect of TNA. In the mixture solution containing H_2O_2, CdY and $S_2O_3^{2-}$, H_2O_2 could reduce $S_2O_3^{2-}$ to S^{2-} by the catalysis of HRP. The generated S^{2-} reacted with CdY to form CdS QDs in situ on the TNAs, improving the PEC performance of TNA under visible light irradiation. The photocurrent would decrease after addition of asulam due to its inhibitory effect towards HRP enzyme activity. Under the optimal experimental conditions, the constructed PEC TNA/HRP biosensor exhibited a satisfying linear range (0.02-2.0 ng mL^{-1}), low limit of detection (4.1 pg mL^{-1}) and good selectivity towards asulam determination, and has been successfully applied for the analysis of real environmental water samples with good precision of RSD less than 6.3% and good accuracy of the recoveries ranged from 90 to 114%.

Accepted manuscript

ACCEPTED MANUSCRIPT

Acknowledgements

This project was supported by the Priority Academic Program Development of Jiangsu Higher Education Institutions, the Top-notch Academic Programs Project of Jiangsu Higher Education Institutions (TAPP), the National Natural Science Foundations of China (21675067), the Science and Technology Project of Xuzhou City (KH17027), and the Natural Science Foundation of Jiangsu Normal University (15XLR007).

References

An, E.M., Shin, H.S., 2011. Food Sci. Biotechnol. 20, 1299-1306.

An, Y.R., Tang, L.L., Jiang, X.L., Chen, H., Yang, M.C., Jin, L.T., Zhang, S.P., Wang, C.G., Zhang, W., 2010. Chem. Eur. J. 16, 14439-14446.

Bradford, M.M., 1976. Anal. Biochem. 72, 248-254.

Chen, D., Zhang, H., Li, X., Li, J.H., 2010. Anal. Chem. 82, 2253-2261.

Chen, Q., Schonherr, H., Vancso, G.J., 2009. Small 5, 1436-1445.

Chen, X., Mao, S.S., 2007. Chem. Rev. 107, 2891-2959.

Chen, Z., Xu, Y.J., 2013. ACS Appl. Mater. Interfaces 5, 13353-13363.

Chicharro, M., Bermejo, E., Ongay, S., Zapardiel, A., 2008. Electroanalysis 20, 534-541.

Chicharro, M., Zapardiel, A., Bermejo, E., Sanchez, A., 2002. Anal. Chim. Acta 469, 243-252.

Chivulescu, A., Catala-Icardo, M., Mateo, J.V.G., Calatayud, J.M., 2004. Anal. Chim. Acta 519, 113-120.

Conrado, R.J., Varner, J.D., Delisa, M.P., 2008. Curr. Opin. Biotechnol. 19, 492-499.

Eskandari, H., Shahbazi-Raz, M., 2016. Turk. J. Chem. 40, 1019-1033.

Accepted manuscript

ACCEPTED MANUSCRIPT

Freeman, R., Willner, I., 2009. Nano Lett. 9, 322-326.

Fu, J.L., Liu, M.H., Liu, Y., Woodbury, N.W., Yan, H., 2012. J. Am. Chem. Soc. 134, 5516-5519.

Ghicov, A., Schmuki, P., 2009. Chem. Commun. 45, 2791-2808.

Jun, Y., Park, J.H., Kang, M.G., 2012. Chem. Commun. 48, 6456-6471.

Kang, U., Park, H., 2013. Appl. Catal. B 140-141, 233-240.

Lai, Y.K., Lin, L.X., Pan, F., Huang, J.Y., Song, R., Huang, Y.X., Lin, C.J., Fuchs, H., Chi, L.F., 2013. Small 9, 2945-2953.

Laviron, E.J., 1979. J. Electroanal. Chem. 101, 19-28.

Li, H., Xing, J., Xia, Z., Chen, J., 2015. Carbon 81, 474-487.

Li, T.L., Lee, W.C., Chang, P.C., Chou, S.S., 2011. J. Food Drug Anal. 9, 40-44.

Li, X., Zhu, J., Li, H.X., 2012. Appl. Catal. B: Environ. 123-124, 174-181.

Liang, Y., Kong, B., Zhu, A.W., Wang, Z., Tian, Y., 2012. Chem. Commun. 48, 245-247.

Liu, M.C., Zhao, G.H., Zhao, K.J., Tong, X.L., Tang, Y.T., 2009. Electrochem. Commun. 11, 1397-1400.

Liu, Y., Du, J.J., Yan, M., Lau, M.Y., Hu, J., Han, H., Yang, O.O., Liang, S., Wei, W., Wang, H., Li, J.M., Zhu, X.Y., Shi, L.Q., Chen, W., Ji, C., Lu, Y.F., 2013. Nature Nanotech. 8, 187-192.

Lu, J.S., Li, H.N., Cui, D.M., Zhang, Y.J., Liu, S.Q., 2014. Anal. Chem. 86, 8003-8009.

Lu, J.S., Shen, Y.F., Liu, S.Q., 2016. Chem. Commun. 52, 7703-7706.

Malashikhina, N., Garai-Ibabe, G., Pavlov, V., 2013. Anal. Chem. 85, 6866-6870.

Muzzarelli, R.A.A., 2009. Carbohyd. Polym. 76, 167-182.

Myland, J.C., Oldham, K.B., 2005. Electrochem. Commun. 7, 282-287.

Nakamura, M., Yasukawa, T., Igarashi, T., Yamada, S., Aizawa, S., 2000. Bunseki Kagaku 41,

Accepted manuscript

ACCEPTED MANUSCRIPT

65-68.

Nouws, H.P.A., Delerue-Matos, C., Lima, J.L.F.C., Garrido, E.M., Vincke, P., Maes, N.A., 2002. J. Environ. Anal. Chem. 82, 69-76.

Ouyang, J.L., Chang, M.L., Zhang, Y.Y., Li, X.J., 2012. Thin Solid Films 520, 2994-2999.

Paramasivam, I., Jha, H., Liu, N., Schmuki, P., 2012. Small 8, 3073-3103.

Pardo-Yissar, V., Katz, E., Wasserman, J.L., Willner, I., 2003. J. Am. Chem. Soc. 125, 622-623.

Roy, P., Berger, S., Schmuki, P., 2011. Angew. Chem., Int. Ed. 50, 2904-2939.

Sanchez, F.G., Diaz, A.N., Bracho, V., Aguilar, A., Algarra, M., 2009. Luminescence 24, 448-452.

Sanchez, F.G., Diaz, A.N., Tellez, C.D., Algarra, M., 2008. Talanta 77, 294-297.

Schoffelen, S., van Hest, J.C.M., 2012. Soft Matter. 8, 1736-1746.

Shangguan, L., Wei, Y.Q., Liu, X., Yu, J.C., Liu, S.Q., 2017. Chem. Commun. 53, 2673-2676.

Song, Y.Y., Schmidt-Stein, F., Bauer, S., Schmuki, P., 2009. J. Am. Chem. Soc. 131, 4230-4232.

Su, C., Shao, C., Liu, Y., 2011. J. Colloid Interface Sci. 359, 220-227.

Subova, I., Assandas, A.K., Icardo, M.C., Calatayud, J.M., 2006. Anal. Sci. 22, 21-24.

Sun, W.T., Yu, Y., Pan, H.Y., Gao, X.F., Chen, Q., Peng, L.M., 2008. J. Am. Chem. Soc. 130, 1124-1125.

Tachikawa, T., Yamashita, S., Majima, T., 2011. J. Am. Chem. Soc. 133, 7197-7204.

Tan, A.W., Pingguan-Murphy, B., Ahmad, R., Akbar, S.A., 2012. Ceram. Int. 38, 4421-4435.

Wang, C.X., Yin, L.W., Zhang, L.Y., Gao, R., 2010. J. Phys. Chem. C 114, 4408-4413.

Wang, H.Y., Wang, G.M., Ling, Y.C., Lepert, M., Wang, C.C., Zhang, J.Z., Li, Y., 2012. Nanoscale 4, 1463-1466.

Accepted manuscript

ACCEPTED MANUSCRIPT

Wang, Q.Y., Yang, X.C., Wang, X.L., Huang, M., Hou, J.W., 2012. Electrochim. Acta 62, 158-162.

Yan, W., Aebersold, R., Raines, E.W., 2009. J. Proteom. 72, 4-11.

Yan, X., Cui, X., Li, B.S., Li, L.S., 2010. Nano Lett. 10, 1869-1873.

Zhang, H., Quan, X., Chen, S., Yu, H.T., Ma, N., 2009. Chem. Mater. 21, 3090-3095.

Zhang, H., Wang, G., Chen, D., Lv, X.J., Li, J.H., 2008. Chem. Mater. 20, 6543-6549.

Zhang, J., Yu, J.G., Jaroniec, M., Gong, J.R., 2012. Nano Lett. 12, 4584-4589.

Zhang, Z.J., Xie, Y.B., Liu, Z., Rong, F., Wang, Y., Fu, D.G., 2011. J. Electroanal. Chem. 650, 241-247.

Highlights

- A sensitive PEC biosensor for asulam due to its enzymatic inhibition to HRP.
- Improvement of PEC performance of TNAs based on enzymatic generation of QD in-situ.
- Good electrochemical and enzymatic property of HRP confined in TNAs.
- Asulam determination with linear range of 0.02-2.0 ng mL^{-1} and LOD of 4.1 pg mL^{-1}.

Accepted manuscript